J. Membrane Biol. 208, 1–14 (2005)
DOI: 10.1007/s00232-005-0814-z

The Journal of
Membrane
Biology

Fast Pseudo-Periodic Oscillation in the Rat Brain Voltage-gated Sodium Channel α Subunit

S. Majumdar, S.K. Sikdar
Molecular Biophysics Unit, Indian Institute of Science, Bangalore 560012, India

Received: 30 June 2005/Revised: 7 November 2005

Abstract. In the work reported here, we have investigated the changes in the activation and fast inactivation properties of the rat brain voltage-gated sodium channel (rNa_v 1.2a) α subunit, expressed heterologously in the Chinese Hamster Ovary (CHO) cells, by short depolarizing prepulses (10 – 1000 ms). The time constant of recovery from fast inactivation (τ_{fast}) and steady-state parameters for activation and inactivation varied in a pseudo-oscillatory fashion with the duration and amplitude of a sustained prepulse. A consistent oscillation was observed in most of the steady-state and non-inactivating current parameters with a time period close to 225 ms, although a faster oscillation of time period 125 ms was observed in the τ_{fast}. The studies on the non-inactivating current and steady-state activation indicate that the phase of oscillation varies from cell to cell. Co-expression of the β1 subunit with the α subunit channel suppressed the oscillation in the charge movement per single channel and free energy of steady-state inactivation, although the oscillation in the half steady-state inactivation potential remained unaltered. Incidentally, the frequencies of oscillation in the sodium channel parameters (4–8 Hz) correspond to the theta component of network oscillation. This fast pseudo-oscillatory mechanism, together with the slow pseudo-oscillatory mechanism found in these channels earlier, may contribute to the oscillations in the firing properties observed in various neuronal subtypes and many pathological conditions.

Key words: Voltage gated sodium channel — Weighted wavelet analysis — Whole-cell patch-clamp — Epilepsy — Oscillation

Introduction

The neuronal voltage-sensitive transient sodium channels are heterotrimeric transmembrane proteins consisting of a channel-forming α subunit and auxiliary β1 or β3 and β2 or β4 subunits (Catterall, 2000; Yu et al., 2003). The voltage-gated sodium channel is needed for the initiation and repetitive firing of action potentials in neurons. Neurons usually undergo adaptation after firing for a few seconds. But in neurological disorders like epilepsy, neurons periodically fire action potentials; the membrane remains in a depolarized state for durations varying from seconds to minutes. The voltage-gated ion channels in neuronal membranes can contribute to the generation of epileptic discharges in the absence of synaptic inputs (Konnerth, Heinemann & Yaari, 1986; Schweitzer, Patrylo & Dudek, 1992; Segal, 1994). The importance of voltage-gated sodium channels in the generation of epileptic discharges and thereby depolarized states of the neuron is suggested by the epilepsy-related mutations that recently have been mapped on the voltage-gated sodium channel α and β1 subunit genes SCN1A, SCN2A and SCN1B (discovery of mutations: Wallace et al., 1998, 2001, 2003; Escayg et al., 2000, 2001: Claes et al., 2001; functional characterization: Alekov et al., 2001; Lossin et al., 2002; Ohmori et al., 2002; Tammaro, Conti & Moran, 2002; Spampanato et al., 2003, Rhodes et al., 2004, to name a few). These mutant channels show variation in the surface expression and altered activation and inactivation properties, leading to either development of a persistent inward current or resulting in the reduction in the β1 modulation of the α subunit channel (Spampanato et al., 2004b), imparting hyperexcitability to the cell (Spampanato et al., 2004a,b). These, together with the fact that veratridine, a sodium-channel modulator, is able to induce epilepsy in case of the wild-type sodium channel itself (Bikson, Barban &

Present address for S. Majumdar, Department of Neuroanatomy, Max Planck Institute for Brain Research, Deutschordenstrasse 46, D-60528 Frankfurt/Main, Germany
Correspondence to: S.K. Sikdar; email: sks@mbu.iisc.ernet.in

Durand, 2002), suggest that certain properties intrinsic to the wild-type sodium channels may be recruited in epileptogenesis. In addition, there is evidence that sodium channels are primarily responsible for sub-threshold membrane potential oscillation (Huangfu & Guyenet, 1997; Kapoor, Li & Smith, 1997; Pape & Driesang, 1998; Amir, Michaelis & Devor, 1999; Desmaisons, Vincent & Lledo, 1999; Wu, Hsiao & Chandler, 2001; Bracci et al., 2003). The aforementioned studies indicate that some underlying molecular mechanism of the sodium channel brings about periodicity in the neuronal activity.

While it is known that epileptic discharge in a single neuron lasts from several milliseconds up to a few minutes (Rutecki & Yang, 1998), the effect of sustained depolarized states of the neuronal membrane on the voltage-gated ion-channel properties has received scant attention. Earlier it has been shown that the time constant of recovery from fast inactivation, τ_{fast}, of the brain voltage-gated sodium channel changes with the duration of a sustained prepulse (Toib, Lyakhov & Marom, 1998; Ellerkmann et al., 2001). However, a relationship between τ_{fast} and prepulse duration could not be concluded. We explored the hypothesis that short prior depolarization (10–1000 ms) causes prepulse duration-dependent oscillatory changes in all the kinetic and steady-state parameters of the activation and fast inactivation properties of the sodium channel, as shown earlier for longer prepulse depolarization (Majumdar, Foster & Sikdar, 2004). The time constant of fast inactivation, steady-state parameters of activation and fast inactivation and non-inactivating current properties of the sodium channel, indeed, evolved in a pseudo-oscillatory fashion with increasing duration and amplitude of the sustained conditioning prepulse. We termed this phenomenon as pseudo-oscillation, because we have observed the oscillatory dependence in a restricted time window (10–1000 ms) and not the entire time range, during which sodium channels can remain depolarized in the normal and/or pathological conditions. Weighted wavelet analysis was employed to detect pseudo-periodic features (Foster, 1996). Interestingly, the β1 subunit suppressed the amplitude of oscillation in the charge movement and the free energy of steady-state inactivation of the α subunit, though it did not alter the intrinsic oscillation evident in the half-inactivation potential. Since oscillation in the single-channel kinetics of the potassium channel is already known (Rahamimoff et al., 1995), our observations indicate that the history-dependent oscillatory properties of the voltage-gated sodium and potassium channels may contribute to the sub-threshold membrane-potential oscillation and epileptic discharges.

Materials and Methods

Electrophysiological Measurements

Whole-cell sodium currents were measured, using the patch-clamp technique, from the rat brain type II A sodium channel (rNa_v 1.2a) α-subunit, stably expressed in CHO cells in our laboratory (CNa18 cells, Sarkar, Adhikari & Sikdar, 1995). CNa18 cells were cultured in DMEM F12 HAM medium (Sigma, St. Louis, MO) with 250 μg/ml geneticin as selection marker to control maximal current expression below 5 nA. For the β1 transient expression in CNa18 cells, the β1 was co-transfected with the green fluorescence protein (EGFP) using Superfect (Qiagen, Germany) at a 2:1 ratio. Only fluorescent cells were patch-clamped in this case after selection with a 20× objective lens, using an inverted fluorescence microscope (Nikon Diaphot TMD, Japan). To be more certain about successful β1 transfection, current from a β1 transfected cell was superimposed on current from a cell transfected with α-subunit alone to look for the significantly faster current indicative of the presence of β1 (Isom et al., 1992). Ionic currents were recorded using an EPC-8 amplifier (HEKA Instruments, Germany). Pipettes for patch-clamp experiments were made from borosilicate glass (Clark Electromedical Instruments, England) using a P97 puller (Sutter Instruments, CA). They were polished to give a resistance of 1 – 3 MΩ, using a microforge setup (List Medical Electronic, Germany). Solutions for patch-clamp recordings were (in mM): 116 CsCl, 10 HEPES, 10 EGTA, 0.5 $CaCl_2$, 15-20 Na^+, pH 7.4 (adjusted with NaOH); and 135 NaCl, 5 HEPES, 1 $MgCl_2$, 1.5 $CaCl_2$, pH 7.4 (adjusted with NaOH), for the pipette and bath solutions, respectively. Experiments were handled with pClamp8.0 (Axon Instruments, Foster City, CA) and Digidata1320 analog-digital converter (Axon Instruments). Data were low-pass filtered at 3–10 kHz and sampled at 16–20 kHz.

Series resistance (*R*s) compensation of 80–90% was applied throughout the recording, and was also routinely monitored before and after acquiring an experimental data set. If the *R*s values varied, the data set was rejected, and the experimental data were acquired again if the *R*s could be controlled to acceptable values by applying suction and an *R*s compensation of 80–90%. Usually, the total time of a single recording varied roughly between 20 s to 8 min, depending on the prepulse duration chosen. Beyond 30 min of recording, many times it became rather difficult to manage series resistance errors, even after applying suction, since the seal became leaky with suction, resulting in anomalous parameter values. Therefore, whenever a problem of leakiness or high series-resistance values (greater than 5 MΩ) arose, the cell was discarded and a new cell was patched. All the recordings were done at 15 °C; the bath temperature was maintained using a PDMI-2 peltier-based microincubator and TC-202 Bi-polar temperature controller (Medical Systems USA). P/4 leak subtraction was done for all sets of experiments. A holding potential of −80 mV was applied throughout, unless otherwise mentioned. Analysis and fitting of the data was done using SigmaPlot 4.0. Data are presented as mean ± SEM.

Modeling

Wavelet analysis was applied on the data sets to unravel the signatures of the pseudo-periodic oscillations in the kinetic and steady-state parameters of the sodium channel. Fast Fourier transformation (FFT) of the data was done using time series (TS, Foster, 1995) and weighted wavelet *z*-transform (WWZ) analysis (Foster, 1996) programs (www.AAVSO.org). WWZ uses the 'wavelet analysis' method to scan the time series data for possible time-variable Fourier components. The F-ratio statistics (WWZ) were calculated to compare the detected Fourier components

obtained by wavelet analysis, to find the statistically significant oscillations present in the data. The advantage of this method over other Fourier transformation methods is that it takes account of the variability in the amplitude of oscillation across the whole data set (such as our data) and allows for little variation in the time period of oscillation, which is usually possible for an experimental data set. The time periods with WWZ scores below 1 were ignored and the values above 1 were plotted. The WWZ statistics are represented for each time-series data in the z-axis of a three-dimensional contour plot, where x- and y- axes represent the duration of the time series and frequency, respectively. In the WWZ contour maps, a concentric circle indicates a peak for a statistically significant oscillation. The WWZ contour maps are presented throughout the text, to represent the time-dependent variation in the oscillatory component and the time period (1/frequency) of the oscillatory components are reported. The data was modelled with the help of the TS program, using the linear slope, variable time periods and amplitudes detected by the WWZ analyses. The modelled curves were regenerated for the data containing statistically significant oscillations only. For FFT and wavelet analysis, frequencies higher than 10 Hz were ignored for prepulse duration dependence, as the lowest sampling interval was 50 ms.

Results

Dependence of τ_{fast} of Recovery on Depolarizing Prepulses

The onset and recovery from fast inactivation have been studied earlier for the rNa$_v$ 1.2a channel α-subunit, expressed in the CHO cell line (Sarkar et al., 1995). To follow the recovery from fast inactivation, cells were pulsed to −10 mV for varying conditioning (prepulse) duration (10 – 1000 ms), followed by a hyperpolarizing recovery pulse step (−90 mV) of varying time (80 such pulses incremented in steps of 1 ms deemed sufficient for studying the recovery from fast inactivation). A test pulse (−10 mV for 10 ms) was applied next, to measure the recovered current. In Fig. 1*A*, a representative recording is shown for 30 ms prepulse duration, along with the pulse protocol. The time constant of recovery from fast inactivation, $\tau_{fast,}$ varies with the prepulse duration in both the prepulse duration ranges 10 – 100 ms and 100 – 1000 ms. In Fig. 1*B*, a plot of the fraction of inactivation ($1-I_n/I_{max}$, where I_n is the current elicited at the nth test pulse and I_{max} is the maximum recovered current) versus recovery time is shown for 10, 50 and 100 ms prepulse depolarization, applied to a single cell. In Fig. 1*C*, the recovered current traces at the test pulse, following 300, 500 and 700 ms prepulse durations, are shown for another cell. Fig. 1*D* shows the plot of the fraction of inactivation versus recovery time for the data in Fig. 1*C*. The data at all prepulse durations were found to be well fitted with a mono-exponential function of the form:

$$F = ae^{-t/\tau} + c \quad (1)$$

where a and c are the initial and final fractions; τ is the time constant. The solid lines in Fig. 1*B* and *D* are the mono-exponential fit of the data. For longer prepulse durations, we compared the fits using mono- and bi-exponential functions. The bi-exponential fit was not found statistically significant over the mono-exponential fit at the 95% confidence level. The τ_{fast} values, corresponding to 10, 50 and 100 ms prepulse depolarization (Fig.1*B*), were 8.01, 11.47 and 14.96 ms, respectively. The τ_{fast} values, corresponding to 300, 500 and 700 ms prepulse durations (Fig. 1*D*), were 21.39, 25.66 and 28.47 ms, respectively. Data from three more cells (indicated as set numbers) are presented in Table 1 to demonstrate the variation in τ_{fast} with prepulse duration. In between two consecutive recordings, cells were held at −80 mV for 1–2 min to ensure complete recovery from fast inactivation. For a single cell, the τ_{fast} does not vary much for a constant prepulse duration, when applied repetitively. For example, when τ_{fast} was measured repetitively from a single cell following 500 ms prepulse duration, τ_{fast} values of 25.29 ms, 24.78 ms and 24.60 ms were obtained, whereas the mean τ_{fast} corresponding to 500 ms prepulse, was 24.24 ± 1.13 ms (total number of observations, $n = 8$). The variation in the τ_{fast} did not depend upon the order in which the prepulse duration was changed. In Table 1, the data is shown for the prepulse durations applied in no particular order, as indicated by the corresponding file names. When a pulse of constant duration was applied repeatedly, similar values of τ_{fast} were obtained. Not all the prepulse durations could be applied to a single cell because of the series resistance variation-related inaccuracies in the measurements, occurring about half an hour after going to the whole-cell configuration. Thus, the nature of prepulse duration-dependent variation in τ_{fast} at all the prepulse durations could not be verified in a single cell.

In the 10–100 ms prepulse duration range with 10 ms sampling interval, the relationship between mean τ_{fast} and prepulse duration appears to be monotonic and follows the power relationship of the form:

$$\tau_{fast} = a\, t^d \quad (2)$$

where, t is the prepulse duration, a is the constant kinetic set point and d is the power. On the other hand, when τ_{fast} is sampled in the 10–1000 ms prepulse duration range with a sampling interval of 50 ms, the curve shows a pseudo-oscillatory trend, topped on a linear slope. The original τ_{fast} values, corresponding to the prepulse duration ranges 10–100 ms and 150–600 ms are presented in Fig. 1*E* and *F*, respectively, along with the mean, to demonstrate the difference in the nature of the curves in these two prepulse duration ranges. In the 150–600 ms prepulse duration range, the τ_{fast} values, corresponding to the

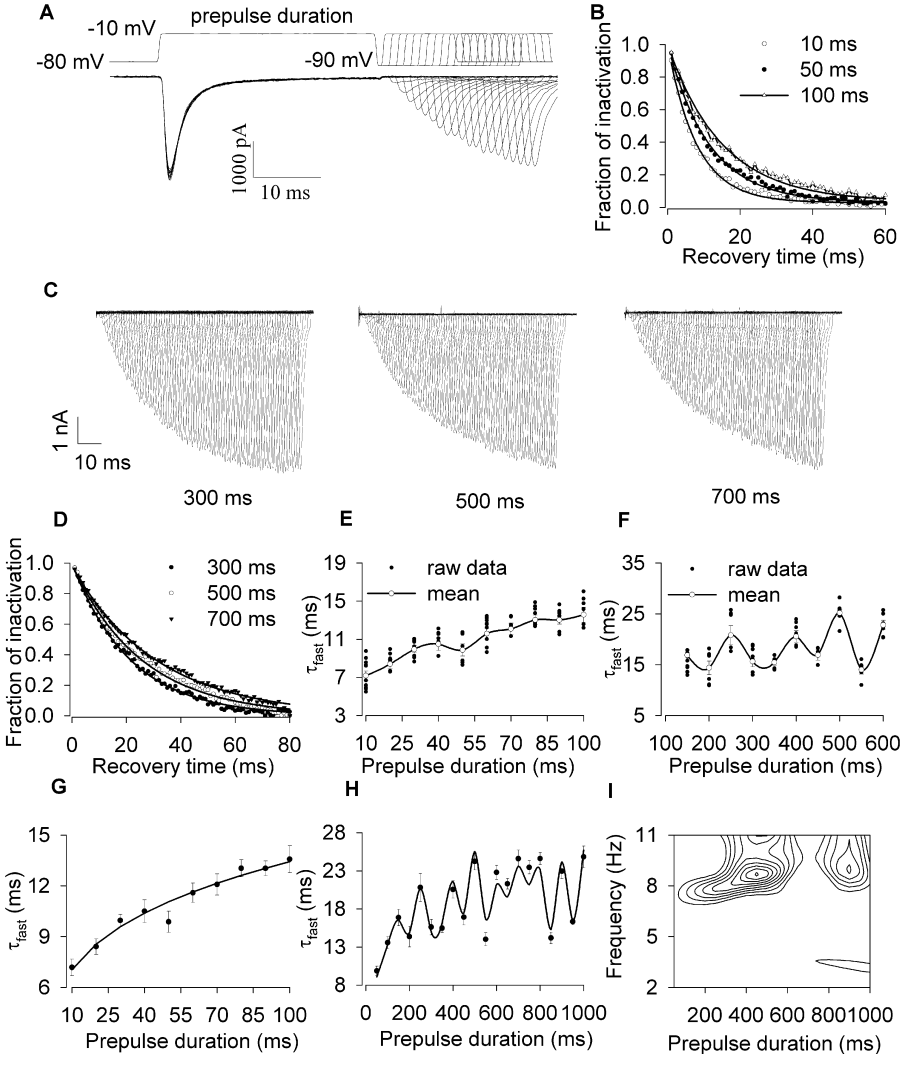

Fig. 1. Recovery from fast inactivation: conditioning prepulse duration and amplitude dependence. (*A*) The upper set of traces shows the protocol used to study recovery from fast inactivation. The current recordings shown correspond to −10 mV conditioning prepulses of 30 ms duration; the recovery potential was −90 mV. (*B*) The fraction of inactivation plotted against recovery time for 10 (○), 50 (●) and 100 ms (Δ) prepulses (−10 mV). The solid lines are the mono-exponential fit with Equation 1. (*C*) The recovered current (at the test pulse) is shown for 300, 500 and 700 ms prepulse durations. The data is from a single cell. (*D*) The fraction of inactivation has been plotted against recovery time for a 300 (●), 500 (○) and 700 ms (▼) prepulse (−10 mV). (*E, F*) Original values of τ_{fast} in two different prepulse duration ranges (10–100 ms and 150–600 ms, respectively) are plotted against prepulse duration along with the respective mean values. The symbols represent data from different cells. The solid lines are the spline lines joining the mean values. (*G*) τ_{fast} plotted against prepulse duration for a 10–100 ms duration range along with the power-law fit (solid line Eq. 2, number of observations, n = 8–12). (*H*) The same plot as *G* is shown for 10–1000 ms prepulse duration range (n = 6–10). The solid line across the data is the model curve generated by the TS program using the variable time period and amplitude indicated in the WWZ contour map (*I*).

peaks of the oscillation, were found to be statistically different from those assuming trough positions (95% confidence level, unpaired *t*-test). The τ_{fast} is plotted against prepulse durations (10–100 ms range) along with the power fit in Fig. 1*G*. The fitted values of the constants are a = 3.75 and d = 0.28. The τ_{fast} data, corresponding to the 10 – 1000 ms duration range, is plotted against prepulse duration in Fig. 1*H*. The weighted wavelet analysis (WWZ) of the data shows presence of a statistically significant oscillation close to a 126.82 ms time period, as indicated by the concentric circles in the corresponding frequency range in the contour map of Fig. 1*I*. The plot also shows a strong modulation of the amplitude of oscillation. It is apparent from the contour plot that the amplitude of oscillation is high in the prepulse duration ranges 100–600 ms and 800–1000 ms, whereas the amplitude of oscillation in the 600–800 ms prepulse duration range is very small, indicated by the absence of WWZ statistics values (less than 1, *see* the modeling section in Materials and Methods) in that range. Such amplitude modulation is observed in the following

Table 1. The τ_{fast} values corresponding to various prepulse durations for three sets of recordings. Each set corresponds to data from a single cell

Set	File name	Prepulse duration (ms)	τ_{fast} (ms)
1	0211cl_7	20	5.91
	0211cl_6	40	7.05
	0211cl_5	60	8.01
	0211cl_4	70	9.42
	0211cl_2	80	9.85
	0211cl_1	90	10.85
	0211cl_10	200	11.13
	0211cl_11	400	18.83
2	3005al_0	350	14.29
	3005al_1	450	14.92
	3005al_2	550	13.51
	3005al_4	850	16.15
	3005al 5	950	17.23
3	1106al_3	750	24.04
	1106al_1	850	13.69
	1106al_0	950	16.59

data sets also. The fitting of the data in Fig 1*H*, using the TS program, indicates that the data contains about 8.5 cycles of oscillation with highly variable amplitude and time period, superimposed on a linear trend with slope 0.0091/ms (the solid line in Fig. 1*H* is the model curve). These results suggest that the τ_{fast} apparently changes with the prepulse duration in a monotonic fashion when measured in a small prepulse duration window (10–100 ms), whereas the intrinsic oscillatory pattern (with time period 128 ms) becomes apparent when the range of prepulse duration is broadened to 10–1000 ms. The data, presented in Fig. 1*G*, represents the first rising phase of the data in Fig. 1*H*. These results also indicate that there is no oscillation faster than that with the time period close to 125 ms in the kinetic properties of the sodium channel.

The prepulse potential dependence of τ_{fast} at 50 ms prepulse duration (Fig. 2*A*) also shows a variable oscillation of period about 21 mV, as shown in the WWZ contour map (Fig. 2*B*). Another signature of oscillation can be seen in the very low frequency region. This very low amplitude oscillation may be evident due to a secondary perturbation of the structure that modulates the main 21 mV oscillation. The solid line across the data in Fig. 2*A* was generated using the TS program. Earlier, prepulse-duration dependence of inactivation time constants was studied in both NaI and NaII sodium channels expressed in *Xenopus* oocytes (Toib et al., 1998) and native rat and human sodium channels (Ellerkmann et al., 2001). These studies could not suggest any suitable model for the apparent non-linear relationship between τ_{fast} and prepulse duration (Ellerkmann et al., 2001) with fewer data points. Our findings suggest that τ_{fast} changes in a pseudo-oscillatory fashion with the duration and amplitude (Fig. 1*H*, 2*A*) of the prepulse depolarization. However, the time period is more than two orders of magnitude faster compared to that of the prepulse duration dependence of the time constant of slow inactivation, as reported before (Majumdar et al., 2004).

Variation in the Steady-State Inactivation Parameters with Conditioning Duration

The steady-state inactivation was studied using the voltage pulse protocol shown in Fig. 3*A*. The cell was pulsed to different step potentials (−120 to 5 mV) for varying conditioning duration (50 – 1000 ms, sampled every 50 ms), immediately followed by a short test pulse (−10 mV for 10 ms). The current, elicited at the test pulse, was normalized with respect to the maximum current for 100 ms and 300 ms conditioning duration and plotted against the conditioning potential in Fig. 3*A*. The conditioning duration dependent change in the fast steady-state inactivation curve can be seen from this plot. The data was fitted with a simple Boltzmann function of the form:

$$p = \frac{1}{1 + e^{(V - V_{half})/k}} \tag{3}$$

where V is the conditioning potential, V_{half} is the half inactivation potential; k is the slope. The charge movement per molecule, z, was estimated by the limiting slope analysis method (Almers, 1978). The V_{half} (Fig. 3*B*) and z (Fig. 3*C*) were found to vary in a non-linear fashion with the conditioning pulse duration. This kind of variation was found to be consistent when tried on single cells. Two such examples are presented in Table 2*a*, where V_{half} and z of fast steady-state inactivation, corresponding to various conditioning pulse durations, are listed for two different cells (indicated by set numbers). It is clear from the table that the variation in the V_{half} and z are not dependent on the order in which the pulse durations were applied. In this case also, all the conditioning durations could not be applied to a single cell. The recordings that had been acquired after half an hour of achieving whole-cell configuration had to be rejected in most instances due to changes in the series resistance that could not be adequately compensated. To examine the resultant effect of conditioning duration on the steady-state distribution of the channels in the fast inactivated state, the change in free energy, ΔG_0 was calculated, where $\Delta G_0 = z\, V_{half}\, F$ (Equ. 4); F is the Faraday constant. ΔG_0 is plotted vs conditioning pulse duration in Fig. 3*D*.

All the data points, except the 250 ms data in Fig. 3*B* and 300 ms data in Fig. 3*C*, apparently fall on a monotonic curve. We did not have reasons to

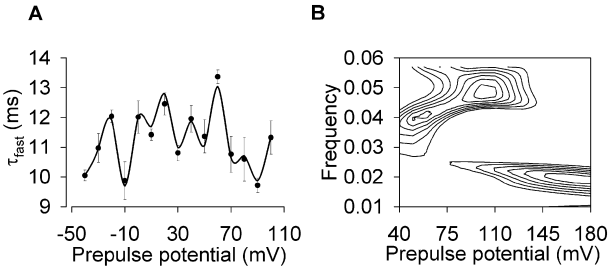

Fig. 2. Prepulse potential dependence of τ_{fast}. (*A*) Prepulse potential dependence (duration, 50 ms) of τ_{fast} is shown along with the model curve (solid line; $n = 6 - 8$). (*B*) WWZ contour map of the data presented in *A*.

ignore these two data points (which deviate from the monotonic curve), as all the original values for these two conditioning durations were consistently coming close to the mean value, as can be made out from the small error bars ($n = 8$ and $n = 11$, for 250 ms duration in Fig. 3*B* and 300 ms duration in Fig. 3*C*, respectively). Plots in Fig. 3*B*, *C* and *D*, indeed, show a strong linear trend superimposed on a pseudo-oscillatory trend, as shown in the WWZ contours of Fig. 3*B*, *C* and *D*. The slope factors were −0.0019/ms, 0.002/ms and −0.0092/ ms and time periods of oscillation were close to 204.87, 228.29 and 228.29 ms for V_{half} *z* and ΔG_0, respectively. These oscillatory components were found to be highly variable in amplitude and time period, although the conditioning duration-dependent oscillatory change in *z* (Fig. 3*C*) is not very pronounced and statistically not very significant (WWZ contour in Fig. 3*C*). The amplitude of oscillation decreases progressively and becomes very small after three cycles of oscillation, in the conditioning duration range 600–800 ms; however, beyond this range, the amplitude of oscillation increases again. The probable reason for such apparently low amplitude oscillation is discussed in the next section of the Results.

Effect of Short Prepulse Duration on the Steady-State Activation Parameters

To examine the effect of short depolarization on steady-state activation, the current-voltage (*I-V*) relationship was obtained before and after a conditioning prepulse of amplitude −10 mV and variable duration (110–1010 ms). A three-pulse protocol was used for this set of experiments. The conditioning pulse preceded a recovery pulse (−80 mV, 10 ms, to allow partial recovery from fast inactivation, so that a macroscopic whole-cell current can be recorded in response to the following pulse), which was followed by the test pulse for the *I-V* relationship (20 ms). The hyperpolarizing leak protocols followed immediately, causing the channels to recover completely from fast

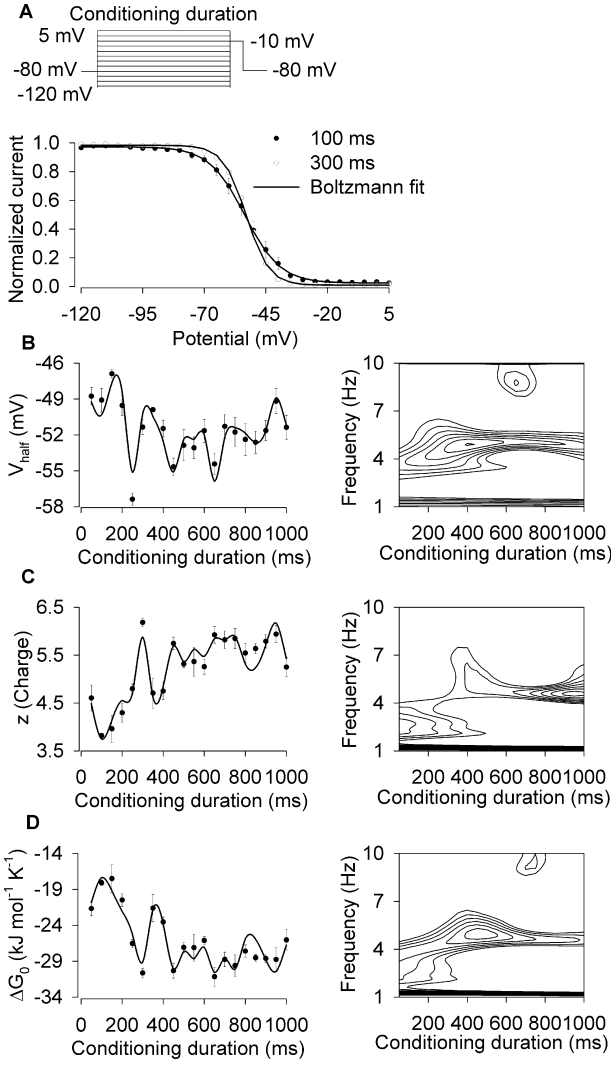

Fig. 3. Steady state inactivation: conditioning-duration dependence. (*A*) The schema above the plot shows the pulse protocol used to study the fast steady state inactivation. The normalized steady state currents at the test pulse are plotted against conditioning potential for 100 ms (●) and 300 ms (○) conditioning duration. (*B, C, D*) The V_{half}, *z* and ΔG_0 values are plotted against conditioning duration ($n = 6 - 10$), along with the WWZ contour maps. The solid lines are the model curves generated by the TS program using the linear slope, variable time period and amplitude of oscillation detected by WWZ analyses.

inactivation. In the next step, the conditioning pulse and the recovery pulse similarly preceded application of the consecutive test pulse that was incremented by 5 mV. The procedure was repeated such that the currents at the test potentials from −70 mV to a final depolarization of 65 mV could be obtained for the *I-V* relationship. The 10 ms duration of −80 mV recovery pulse was adjusted to the conditioning duration later, such that the resultant conditioning duration range became 100–1000 ms. After every recording, the patch was held at −80 mV holding

Table 2. (a) Fast steady-state inactivation parameters from a single cell, at different conditioning durations

Set number	File name	Conditioning duration ms	V_{half} mV	z charge
1	2511bl_21	100	−47.31	3.82
	2511bl_17	200	−50.21	4.84
	2511bl_13	400	−52.13	4.58
	2511bl_8	600	−51.61	5.23
	2511bl_7	700	−52.31	6.32
	2511bl_4	800	−49.59	5.00
	2511bl_19	900	−54.68	5.40
2	2711al_11	600	−55.44	4.95
	2711al_9	700	−53.95	4.99
	2711al_5	900	−52.52	5.40
	2711al_7	1000	−53.18	5.30

Table 2. (b) Fast steady-state activation parameters from a single cell, at different conditioning durations

Set number	Conditioning duration ms	V_{half} mV	z charge
1. Control values:	100	−10.2700	4.4030
V_{half} = −15.7400 mV	200	−9.7040	4.1090
z = 5.6370 e	300	−10.2300	3.7980
	700	−11.9800	4.3830
	800	−10.8700	3.8030
	900	−10.6900	4.0780
	1000	−9.5250	3.5850
2. Control values:	400	−8.7320	3.3490
V_{half} = −15.8700 mV	500	−13.4500	3.5630
z = 5.1760 e	600	−11.3300	2.6680
3. Control values:	400	−13.8200	4.5780
V_{half} = −18.0200 mV	500	−14.1400	4.0120
z = 6.2690 e	600	−16.2000	3.8430

potential for 1–2 min to ensure complete recovery from the effect of applied prepulse duration. The currents for control and after 300 ms prepulse duration are compared in Fig. 4*A*; the protocol is also shown. In Fig. 4*B* and 4*C*, *I-V* plots and the normalized conductances for the recordings in Fig. 4*A* are compared. The solid lines in Fig. 4*C* are the Boltzmann fit (Equation 3) to the data. A depolarizing shift in the steady-state activation (V_{half}) and a reduction in charge movement during activation (z) were observed on applying conditioning depolarization (Fig. 4*D*) at all prepulse durations. For the data presented in Fig. 4*A*, *B* and *C*, fitted values of V_{half} and z were −13.120 mV, 6.195e for control and −9.085 mV, 4.667e after 300 ms depolarization to −10 mV, respectively. The V_{half} and z were found to vary with the prepulse duration in an oscillatory manner, as shown in Fig. 4*D* and *E*, respectively, where the data from three individual cells are plotted. The lateral shift in the plots is due to the fact that the control values (corresponding to the 0 ms prepulse duration in the plots) of V_{half} and z varied a bit from cell to cell. The difference in the phase of oscillation is also noted, though the overall time periods of oscillation are close to 200–250 ms.

It was shown earlier that the decrease in G_{max} (maximal conductance during activation) causes a decrease in the charge movement of activation (Q_{max}) in a linear fashion (Sheets & Hanck, 1999; Sheets et al., 1999) in cardiac sodium channels. Hence, the G_{max} may also vary with prepulse duration in an oscillatory fashion, assuming Q_{max} varies with prepulse duration in an oscillatory manner, as Q_{max} is directly proportional to z ($Q_{max} = Nz$, N is the maximal number of channels that can be opened on depolarization). However, G_{max} was found to change monotonically with prepulse duration, indicating that the non-linear decrease in z with prepulse duration is not an effect of decrease in G_{max}. To demonstrate this, the G_{max} for an individual cell is plotted against prepulse duration in Fig. 4*F*, where the solid line is the mono-exponential fit with Equation 1; τ = 443.25 ms. This monotonic behavior probably indicates the entry of the channel in an intermediate inactivated state, a separate inactivated state that has been reported before (Toib et al., 1998). A direct measurement of the Q_{max} could not be done because of the very small amplitude of gating current. Figure 4*G* presents families of *I-V* plots for the same data set shown in Fig. 4*F*. This plot shows that

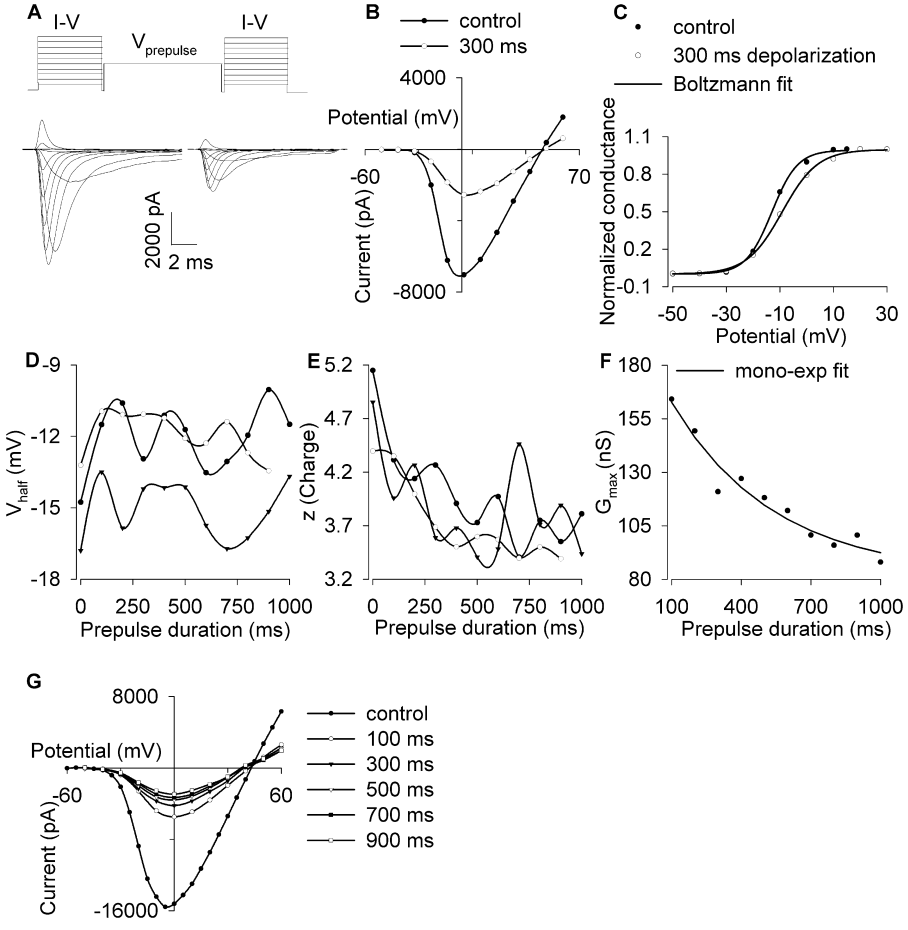

Fig. 4. Steady-state activation: conditioning prepulse duration dependence. (*A*) Each pulse of the *I-V* protocol was applied before and after the prepulse to −10 mV, as shown here (*see* Results section for details). The currents are presented for control and after a 300 ms prepulse to −10 mV. (*B*, *C*) The *I-V* and normalized conductance plots are shown for the data presented in ***A***. Solid lines in ***C*** are the Boltzmann fits. (*D*, *E*) V_{half} and z are plotted against prepulse duration for three different cells. (*F*) G_{max} from a single cell is plotted against the prepulse duration along with the mono-exponential fit (solid line). (*G*) Family of *I-V* plots following prepulses of different durations are shown together for the same cell as in *D*, *E* (●), *F*.

reversal potential for all the recordings did not vary significantly (1–3 mV), and the effect of prepulse duration on the steady-state activation parameters cannot be attributed to changes in leak current and/or series resistance problems. The seal resistance (close to 2 GΩ) was comparable for all the recordings presented in Fig. 4*D* to *F*.

Though both the V_{half} and z show signatures of oscillation close to 200 – 250 ms for the data sets from individual cells presented in Fig. 4*D* and *E*, respectively, the phase of oscillation in V_{half} and z with prepulse duration was found to vary among the cells. This contributed to the large error bars of V_{half} and z values when the results from several cells were pooled together to calculate the mean changes in V_{half} and z with prepulse duration. The mean ΔV_{half}, Δz and $\Delta\Delta G_0$ with respect to control are plotted against the prepulse duration in Fig. 5*A*, *C* and *E*, respectively. Signatures of oscillation or pseudo-oscillation in mean ΔV_{half}, Δz and $\Delta\Delta G_0$ are seen in WWZ contours of Fig. 5*B*, *D* and *F*, respectively. Figure 5*C* shows a linear trend as well, with slope −0.00032/ms. The time periods of oscillation are 723.63 ms for ΔV_{half} (Fig. 5*A*), 256.77 ms for Δz (Fig. 5*C*) and 241.21 ms for $\Delta\Delta G_0$ (Fig. 5*E*). The solid lines in Fig. 5*A*, *C* and *E* are the model curves generated by the TS programme using the statistically significant oscillations detected by the WWZ analyses. The phase differences in oscillation in V_{half} across the cells gives rise to the anomalous time period of 723.63 ms for $\Delta V_{half,}$ although the time periods of mean Δz and $\Delta\Delta G_0$ do not get affected much by the averaging procedure, except for a compromise in the amplitude of oscillation. This inherent phase difference of oscillation across the cells is also probably the cause of the low amplitudes of oscillation found in the fast steady-state inactivation parameters (Fig. 3*B*, *C*, *D*).

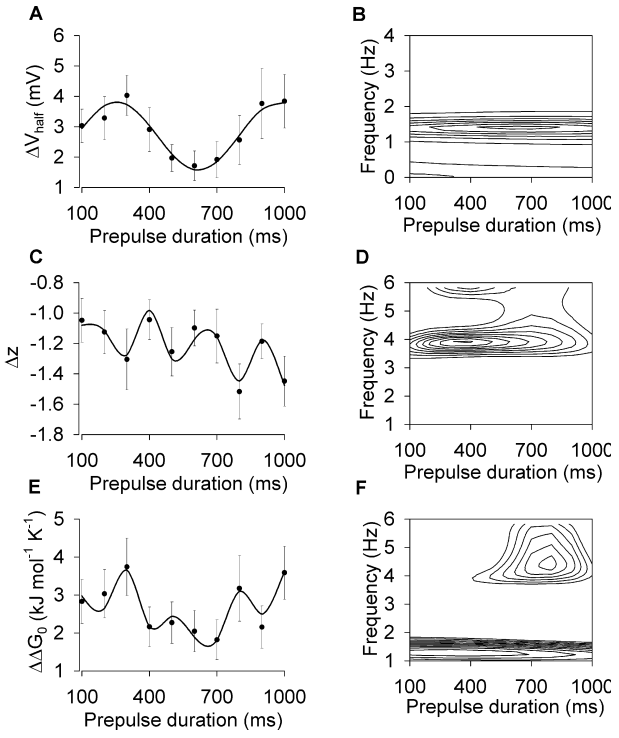

Fig. 5. Oscillation in steady-state activation parameters. (*A*, *C*, *E*) Changes in V_{half}, z and ΔG_0, with respect to control, are plotted against the prepulse duration. (*B*, *D*, *F*) WWZ contours of V_{half}, z and ΔG_0, respectively (n = 6–8). The solid lines in *A*, *C*, *E* are the model curves generated by the TS programrm using the slope, variable time period and amplitude of oscillation detected by WWZ analyses.

Variation in the Non-Inactivating Component of the Sodium Current with Prepulse Duration

The finite, non-inactivating component of sodium current (Magistretti & Alonso, 1999) can amplify small depolarization and sustain repetitive firing in a neuron. Results of Figs. 3, 4 and 5 suggest that both the steady-state activation (m_∞) and steady-state inactivation (h_∞) properties of the sodium channel vary with the prepulse duration in an oscillatory manner. This indicates that the non-inactivating fraction of current may also show prepulse-duration dependence. To measure the non-inactivating fraction of current, the cells were subjected to a fast voltage ramp of 3 mV/ms, preceded by a prepulse of −10 mV of variable duration (100–1000 ms), from a holding potential of −80 mV. The protocol and the non-inactivating current, elicited after 100 ms prepulse duration, are shown in Fig. 6*A*. The non-inactivating current component is shown at a higher magnification in the adjacent panel. Fig. 6*B* shows the variation in non-inactivating current properties with prepulse duration for a single cell. In this case, the peak of non-inactivating current has shifted for 600 ms prepulse duration with respect to 400 ms and 700 ms prepulse durations. The peak potential, i.e., the potential at which the peak of the non-inactivating current is observed and the relative change in the peak non-inactivating current with respect to the current at the beginning of the prepulse (*see* Fig. 6*A*) are plotted in Fig. 6*C* and *D*, respectively, for four individual cells. The prepulse duration was changed in an ascending order for the recordings done with cells 1 and 2, whereas prepulse duration was changed in a random order for recordings with cells 3 and 4. In between two consecutive recordings, the patch was held at −80 mV for 1–2 min, to ensure complete recovery from the effect of previous prepulse depolarization. In all the cases, pseudo-oscillation is evident for both peak potential and relative peak current. Additionally, relative peak current shows a strong linear trend. However, the phase of oscillation is found to vary strongly from cell to cell, such that there is hardly any overlap of the traces. Hence, averaging of the data was not done for this set of experiments. The series resistance was cautiously monitored and compensated in between two consecutive recordings for each cell. In all the recordings, leak current was extremely small (gigaseal) and comparable. Hence, the phase difference across the cells is not attributable to experimental errors. A lateral shift in the peak potential curve is observed from cell to cell (Fig. 6*C*). This is probably because the half-activation potential for control sodium current varied from one cell to the other.

Weighted wavelet analysis of the peak potential of all the four data sets (Fig. 6*C*) reveals a significant oscillation of time period 275.14 ± 7.77 ms (n = 4, the four cells in Fig. 6*C*). In addition, a linear component of variable slope factors was also found. The WWZ F-statistics contour is plotted in Fig. 6*E* for the peak potential of cell 4. All the plots in Fig. 6*D*, corresponding to relative amplitude of peak non-inactivating current, showed a very strong linear trend with the slope factor ranging from −0.000029/ms to −0.000045/ms. In addition, they showed the presence of moderate to very low amplitude oscillation around time period 245.09 ± 3.89 ms (n = 4). These subtle changes in the non-inactivating current as a result of variation in peak current amplitude and peak potential with prepulse duration may influence the firing pattern of a neuron, giving rise to periodic activity.

Effect of the β1 Subunit on the Oscillatory Nature of Conditioning-Duration Dependence of Steady-State Inactivation Parameters

To examine the effect of an auxiliary subunit on the observed periodicity associated with the properties of the α subunit of the sodium channel, the β1 subunit was transiently expressed in CHO carrying the rNa$_v$1.2a α subunit. The activation and inactivation of α + β1 channels are significantly faster compared to α

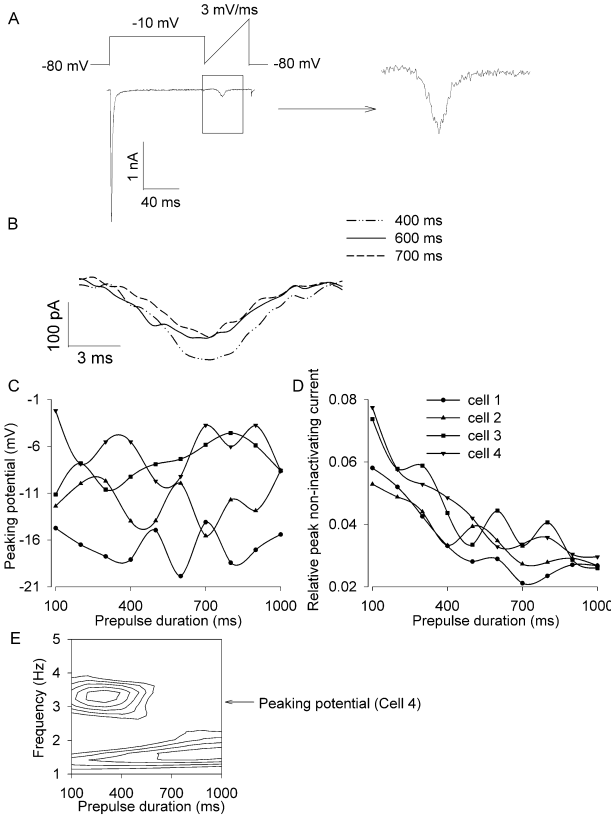

Fig. 6. Variation of non-inactivating current with prepulse duration. (*A*) Plot of non-inactivating current following 100 ms prepulse duration to −10 mV is shown along with the voltage pulse protocol. The non-inactivating current region has been magnified to show the non-inactivating current at greater resolution. (*B*) Non-inactivating currents from a single cell are shown for comparison. The data correspond to 400, 600 and 700 ms prepulse durations. (*C*, *D*) The peaking potential and peak normalized non-inactivating current are plotted against the prepulse duration for four cells to demonstrate the pseudo-periodic nature. (*E*) The WWZ contour map of peaking potential of cell 4 is shown.

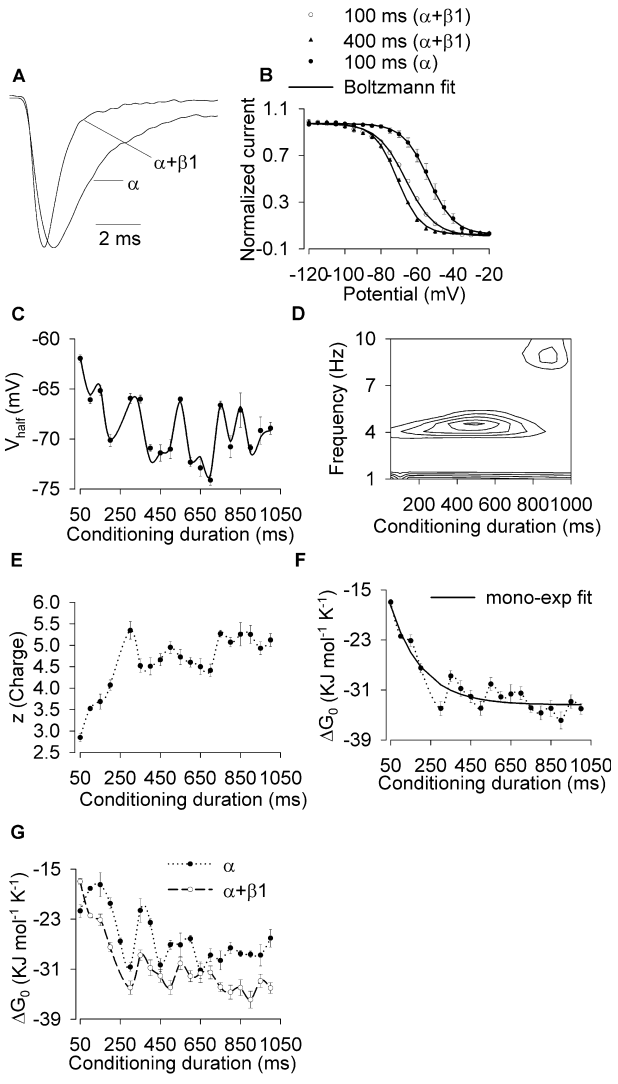

Fig. 7. Effect of β1 subunit on the periodicity of steady state inactivation parameters. (*A*) The normalized currents from α and α+β1 channels following step depolarization to −10 mV are superimposed. (*B*) The steady-state inactivation data for 100 ms (○) and 400 ms (▲) prepulse shown for α + β1 along with the 100 ms data for α (●). The solid lines through the data points are the Boltzmann fits. (*C*, *E*, *F*) V_{half}, z and ΔG_0 of α + β1 are plotted against the prepulse duration, respectively (n = 7–10). (*D*) WWZ contour of the data shown in *C*. The solid line in *C* is the model curve generated using the TS programme. In *F*, the solid line is the mono-exponential fit. (*G*) Comparison of ΔG_0 form the α and α + β1 channel.

alone, the effect on inactivation being more pronounced (τ_{fast} is 1.06 ± 0.06 ms, n = 20 for α + β1 and 1.63 ± 0.08 ms, n = 18 for α), as shown in Fig. 7*A*. The predominant effect of the β1 subunit on the inactivation properties of the channel corroborates earlier findings (Isom et al., 1992, 1995). Though, the extent of change in τ_{fast} strongly depended on the expression system (Isom et al., 1995), the effect on steady-state inactivation was found to be independent of the expression system chosen. This led us to specifically examine the effect of the β1 subunit on the prepulse duration-dependent change in the steady-state inactivation parameters of the α subunit containing sodium channel. An about 20 mV hyperpolarizing shift was observed in the steady-state inactivation curve in presence of β1, as shown in Fig. 7*B* where data corresponding to 100 ms conditioning duration for a and α + β1 channels are compared (protocol is shown in Fig. 3*A*). Variation in the steady-state inactivation parameters, V_{half} and z was observed with conditioning duration for the α + β1 channel, similar to α channel alone (*see* Fig. 3*A*). The data is shown in Fig. 7*B* where the effect of 100 ms and 400 ms conditioning duration on steady-state inactivation is compared. The solid lines are the Boltzmann fit to the data. Variation in V_{half}, z and ΔG_0 with conditioning duration are shown for α + β1 in Fig. 7*C*, *E* and *F*, respectively. While WWZ analysis suggests an oscillation with a time period of

about 242.39 ms and a slope factor of-0.0052/ms for conditioning-duration dependence of V_{half} (Fig. 7*C*), data corresponding to z and ΔG_0 are largely monotonic (mono-exponential fit is shown in Fig. 7*F*, solid line). The data for ΔG_0 of α and α + β1 channels are compared in Fig.7*G*, where suppression of oscillation in ΔG_0 in presence of β1 subunit is clearly discernible. However, periods of oscillation in V_{half} for α and α + β1 are comparable (compare Figs. 3*B* and 7*C*). This indicates that the auxiliary β1 subunit interacts with a key part of the channel core, which is responsible for rendering periodicity to the charge movement during inactivation but not to the half-inactivation potential. A recent report (Spampanato et al., 2004b) shows that an epilepsy-related mutation in the C-terminus of the sodium channel α subunit causes weaker modulation by the β1 subunit, rendering hyperexcitability to the cells. A reduction in β1 interaction with α might increase the amplitude of oscillation in the inactivation parameters also (Fig. 7*G*), causing higher tendency to have periodic burst activity in the diseased condition.

Discussion

Though the biological membrane gets displaced on depolarization (Zhang, Keleshian & Sachs, 2001), there is no evidence for physical oscillation of the membrane causing indirect changes in the channel's kinetic properties upon depolarization. Further, the sodium channel α subunit is tethered to the cytoskeleton, and changes in the cytoskeleton structure alter surface expression of the channel (Komada & Soriano, 2002). Modulation of the kinetic and steady-state properties of the brain sodium channel by mechanical destabilization of the cytoskeletal tethering was shown for human brain sodium channel α subunit, expressed in *Xenopus* oocytes (Shcherbatko et al., 1999). The effect of cytoskeleton disruption was found to be equivalent to the effect of β1 subunit on the properties of the α subunit of the channel. However, it is difficult to assume at this point that the oscillation, seen in all the kinetic and steady-state properties of the sodium channel, takes place because of the oscillatory disturbance of the cytoskeleton, as there is no such evidence to date for oscillatory disturbance of the cytoskeleton. The prepulse durations, applied in our study, are much shorter compared to the time scale of the endogenous PKA/PKC/G-protein activation-related modulation of the sodium channel (Li et al., 1993; Ma et al., 1994). Also, since we did not include phosphorylating compounds like cAMP/ATP in our internal solution a long-term modulation of the sodium channel by signal transduction molecules should not take place due to the dialysis of the cell with the internal solution. Hence, the dependence of the oscillatory mechanism on the duration of prepulse depolarization may be independent of the phosphorylation states of the channel molecule. Thus, the fast pseudo-oscillation, similar to the slow oscillations in these channels shown before (Majumdar et al., 2004), appears to be an intrinsic property of the sodium channel. The pseudo-oscillatory changes in the properties of the non-inactivating component of the sodium current (Fig. 6) indicate that this property may lead to periodic changes in neuronal excitability as well. There is evidence that suggests the role of voltage-gated sodium and potassium channels in the sub-threshold membrane potential oscillations (Boehmer et al., 2000); slow oscillation in the single-channel kinetics of the potassium channel was also observed (Rahamimoff et al., 1995). Thus, periodic patterns associated with sub-threshold oscillations in the membrane potential and epileptic discharge in neurons might have major contributions of the intrinsic pseudo-oscillatory properties of the voltage-gated sodium and potassium channels. However, this will strongly depend on the difference in the phase of oscillation in these two types of voltage-gated ion channels.

The modelling of the periodic changes was done with a combination of a linear (that is, a monotonic term) and a variable oscillatory term in most of the cases. The increasing (in Fig. 1*H*) or decreasing (in Fig. 3*D*) monotonic nature of the line joining the peak/trough points of the data can be due to the fact that the rising or falling phase of the slower oscillation (with time period $\sim$ 30–40 s, Majumdar et al., 2004) is coincident with the faster oscillation. Thus, the apparent monotonic term can be due to the concurrence of slow oscillation (Majumdar et al., 2004) with fast oscillation. The time-dependent variation of the amplitude of oscillation indicates that there are additional molecular processes that affect the oscillatory mechanism in a time-dependent manner. It is quite probable that a single physical structure in the molecule does not undergo time-dependent oscillation in actuality. Continuous molecular rearrangement takes place during channel activation and inactivation, because of which the resultant energy of the conformations changes dynamically in an oscillatory energy landscape (Figs. 3*D*, 5*E*).

In principle, an oscillatory pattern can be generated by a combination of exponential processes with different time constants. Activation and fast inactivation processes are exponential processes having unequal rate constants; coupling of these processes was also observed in this channel earlier (Wang & Wang, 1997; Mitrovic, George & Horn, 1998). Thus, it is quite probable that the activation and inactivation processes couple optimally, resulting in the fast and slow pseudo-periodic oscillations in the channel's kinetic and steady-state parameters. As the majority of the steady-state activation and steady-

state inactivation parameters show a consistent oscillation near a 250 ms time period, this further strengthens the hypothesis that coupling between activation and fast inactivation underlies the apparent pseudo-oscillatory pattern. Alternatively, the single channels interact with each other in a suitable way, directly or indirectly through a signal transduction machinery, to give rise to pseudo-oscillatory whole-cell properties. A systematic study of the single-channel properties of the sodium channel would probably throw more light on the underlying mechanism of pseudo-oscillation.

Surprisingly, the phase of pseudo-oscillation was found to vary from cell to cell when the effect of prepulse duration on the steady-state activation and non-inactivating current properties was studied. It appears that the phase of oscillation for each cell is a time-independent parameter and is characteristic for each cell, since the phase information is not restored to a fixed value when cells were held at −80 mV holding potential for several seconds in between recordings. Alternatively, the phase information varies with a very long time period such that it appears to be constant within the total recording time (maximum 45 minutes). Care was taken to avoid experimental artifacts. All the measurements were done at a constant low temperature (15°C) to slow the channel kinetics for accurate estimations of the biophysical parameters. It is difficult to pin-point the reason for the variability in the phase information across the cells at this stage. The data does not indicate that the sodium channel itself is responsible for such variability in the phase information. Probably, a higher-order structure or a signaling cascade contributes to this process. The variable phase information among different cells confers a higher level of history dependence to the cell. The periodic changes in the peak potential and the relative amplitude of peak non-inactivating current with prepulse duration observed in this channel should cause periodic change in the firing pattern of a neuron.

Interestingly, though co-expression of auxiliary β1 subunit suppressed oscillation in the charge movement during steady-state inactivation, the oscillation in half steady-state inactivation potential remained almost unaltered (compare Figs. 3*B* and 7*C*). This indicates that the β1 subunit interacts with a key part of the channel-forming α subunit that is responsible for the observed pseudo-periodic oscillation in the charge movement, associated with the steady-state inactivation. Although experimental studies to confirm the pseudo-oscillatory mechanism in the native voltage-gated sodium channels are yet to be done, the existence of such a mechanism is a distinct possibility. Incidentally, the frequency of the fast oscillation in the sodium channel parameters (4–8 Hz) is comparable to the frequency of theta oscillations (5–8 Hz) found in the EEG recordings from the cortex and the hippocampus in normal (for example, Nishida et al., 2004, Yamaguchi et al., 2004) and pathological (Clemens, 2004) conditions. Thus, the synchronized network oscillation may have contributions of the sodium channel's intrinsic oscillatory properties as well. Many epilepsy-related mutations were either mapped in the vicinity of the voltage sensor and pore-forming domains (Kearney et al., 2001; Spampanato et al., 2001; Claes et al., 2003; Rhodes et al., 2004), the structure responsible for the charge movement across the membrane during voltage-dependent gating, or the structure that is responsible for the α and β1 subunit interaction (Spampanato et al., 2004b). Our data, presented here, indicates that: 1) pseudo-periodicity in the charge movement during channel gating can be exploited in wild-type or mutant sodium channels to induce periodic bursts of action potentials; 2) a lack of β1 modulation of a channel will increase the amplitude of oscillation (Fig. 7*G*), imparting higher propensity for such periodic bursts of action potentials. Hence, more information on the mechanism of pathological hyperactivity can be derived by looking into the prepulse dependence of the properties of the physiologically relevant mutant sodium channels. Recent simulation studies on the epilepsy-related mutations in the sodium channel indicate that the mutated channels impart hyperexcitability to the neurons (Spampanato et al., 2004a, b). By combining this information with our observation, one can speculate that intrinsic oscillation in sodium channel properties should be capable of generating synchronized oscillatory activity in normal conditions (when cells have the same phase history); the disease-associated mutations render hyperexcitability to the cells, probably by increasing the amplitude of the non-inactivating current (Rhodes et al., 2004), that would prolong the spontaneous firing activity in pathological conditions.

We acknowledge Dr. G. Foster for discussions, Prof. W.A. Catterall for providing the β1 subunit clone and K.V. Jagadeesh and K. Karlin Raja for their help in β1 subunit molecular biology. The research was supported by funds from the Department of Science and Technology, India, and SRF from C.S.I.R., India to S.M.

References

Alekov, A.K., Rahman, M.M., Mitrovic, M., Lehmann-Horn, F., Lerche, H. 2001. Enhanced inactivation and acceleration of activation of the sodium channel associated with epilepsy in man. *Eur. J. Neurosci.* **13:**2171–2176

Almers, W. 1978. Gating currents and charge movements in excitable membranes. *Rev. Physiol. Biochem. Pharmacol.* **82:**96–190

Amir, R., Michaelis, M., Devor, M. 1999. Membrane potential oscillations in dorsal root ganglion neurons:role in normal electrogenesis and neuropathic pain. *J. Neurosci.* **19:**8589–8596

Bikson, M., Barban, S.C., Durand, D.M. 2002. Conditions sufficient for nonsynaptic epileptogenesis in the CA1 region of hippocampal slices. *J. Neurophysiol.* **87:**62–71

Boehmer, G., Greffrath, W., Martin, E., Hermann, H. 2000. Subthreshold oscillation of the membrane potential in magnocellular neurones of the rat supraoptic nucleus. *J. Physiol.* **526:**115–128

Bracci, E., Centonze, D., Bernardi, G., Calabresi, P. 2003. Voltage-dependent membrane potential oscillations of rat striatal fast-spiking interneurons. *J. Physiol.* **549:**121–130

Catterall, W.A. 2000. From ionic currents to molecular mechanisms: the structure and function of voltage-gated sodium channels. *Neuron* **26:**13–25

Claes, L., Ceulemans, B., Audenaert, D., Smets, K., Lofgren, A., Del-Favero, J., Ala-Mello, S., Basel-Vanagaite, L., Plecko, B., Raskin, S., Thiry, P., Wolf, N.I., Van Broeckhoven, C., De Jonghe, P. 2003. De novo SCN1A mutations are a major cause of severe myoclonic epilepsy of infancy. *Hum. Mutat.* **21:**615–21

Claes, L., Del-Favero, J., Ceulemans, B., Lagae, L., Van Broeckhoven, C., De Jonghe, P. 2001. De novo mutations in the sodium-channel gene SCN1A cause severe myoclonic epilepsy of infancy. *Am. J. Hum. Genet.* **68:**1327–1332

Clemens, B. 2004. Pathological theta oscillations in idiopathic generalised epilepsy. *Clin. Neurophysiol.* **115:**1436–41

Desmaisons, D., Vincent, J.D., Lledo, P.M. 1999. Control of action potential timing by intrinsic sub threshold oscillations in olfactory bulb output neurons. *J. Neurosci.* **19:**10727–10737

Ellerkmann, R.K., Riazanski, V., Elger, C.E., Urban, B.W., Beck, H. 2001. Slow recovery from inactivation regulates the availability of voltage-dependent Na(+) channels in hippocampal granule cells, hilar neurons and basket cells. *J. Physiol.* **532:**385–397

Escayg, A., Heils, A., MacDonald, B.T., Haug, K., Sander, T., Meisler, M.H. 2001. A novel SCN1A mutation associated with generalized epilepsy with febrile seizures plus–and prevalence of variants in patients with epilepsy. *Am. J. Hum. Genet.* **68:**866–873

Escayg, A., MacDonald, B.T., Meisler, M.H., Baulac, S., Huberfeld, G., An-Gourfinkel, I., Brice, A., LeGuern, E., Moulard, B., Chaigne, D., Buresi, C., Malafosse, A. 2000. Mutations of SCN1A, encoding a neuronal sodium channel, in two families with GEFS+2. *Nat. Genet.* **24:**343–345

Foster, G. 1995. The Cleanest Fourier Spectrum. *Astronom. J.* **109:**1889–1902

Foster, G. 1996. Wavelets for period analysis of unevenly sampled time series. *Astronom. J.* **112:**1709–1729

Huangfu, D., Guyenet, P.G. 1997. Autoactivity of A5 neurons: role of sub threshold oscillations and persistent Na^+ current. *Am. J. Physiol.* **273:**H2280–H2289

Isom, L.L., De Jongh, K.S., Patton, D.E., Reber, B.F., Offord, J., Charbonneau, H., Walsh, K., Goldin, A.L., Catterall, W.A. 1992. Primary structure and functional expression of the beta 1 subunit of the rat brain sodium channel. *Science* **256:**839–842

Isom, L.L., Scheuer, T., Brownstein, A.B., Ragsdale, D.S., Murphy, B.J., Catterall, W.A. 1995. Functional co-expression of the beta 1 and type IIA alpha subunits of sodium channels in a mammalian cell line. *J. Biol. Chem.* **270:**3306–3312

Kapoor, R., Li, Y.G., Smith, K.J. 1997. Slow sodium-dependent potential oscillations contribute to ectopic firing in mammalian demyelinated axons. *Brain* **120:**647–652

Kearney, J.A., Plummer, N.W., Smith, M.R., Kapur, J., Cummins, T.R., Waxman, S.G., Goldin, A.L., Meisler, M.H. 2001. A gain-of-function mutation in the sodium channel gene Scn2a results in seizures and behavioral abnormalities. *Neuroscience* **102:**307–317

Komada, M., Soriano, P. 2002. [Beta]IV-spectrin regulates sodium channel clustering through ankyrin-G at axon initial segments and nodes of Ranvier. *J. Cell. Biol.* **156:**337–348

Konnerth, A., Heinemann, U., Yaari, Y. 1986. Nonsynaptic epileptogenesis in the mammalian hippocampus in vitro. I. Development of seizure like activity in low extracellular calcium. *J. Neurophysiol.* **56:**409–423

Li, M., West, J.W., Numann, R., Murphy, B.J., Scheuer, T., Catterall, W.A. 1993. Convergent regulation of sodium channels by protein kinase C and cAMP-dependent protein kinase. *Science* **261:**1439–1442

Lossin, C., Wand, D.W., Rhodes, T.H., Vanoye, C.G., George, A.L. Jr 2002. Molecular basis of an inherited epilepsy. *Neuron* **34:**877–884

Ma, J.Y., Li, M., Catterall, W.A., Scheuer, T. 1994. Modulation of brain Na^+ channels by a G-protein-coupled pathway. *Proc. Natl. Acad. Sci. USA* **91:**12351–12355

Magistretti, J., Alonso, A. 1999. Biophysical properties and slow voltage-dependent inactivation of a sustained sodium current in entorhinal cortex layer-II principal neurons: a whole-cell and single-channel study. *J. Gen. Physiol.* **114:**491–509

Majumdar, S., Foster, G., Sikdar, S.K. 2004. Induction of pseudo-periodic oscillation in voltage gated sodium channel properties is dependent on the duration of prolonged depolarization. *Eur. J. Neurosci.* **20:**127–143

Mitrovic, N., George, A.L. Jr., Horn, R. 1998. Independent versus coupled inactivation in sodium channels-role of the domain 2 S4 segment. *J. Gen. Physiol.* **111:**451–462

Nishida, M., Hirai, N., Miwakeichi, F., Maehara, T., Kawai, K., Shimizu, H., Uchida, S. 2004. Theta oscillation in the human anterior cingulate cortex during all-night sleep: an electrocorticographic study. *Neurosci. Res.* **50:**331–41

Ohmori, I., Ouchida, M., Ohtsuka, Y., Oka, E., Shimizu, K. 2002. Significant correlation of the SCN1A mutations and severe myoclonic epilepsy in infancy. *Biochem. Biophys. Res. Commun.* **295:**17–23

Pape, H.C., Driesang, R.B. 1998. Ionic mechanisms of intrinsic oscillations in neurons of the basolateral amygdaloid complex. *J. Neurophysiol.* **79:**217–226

Rahamimoff, R., Edry-Schiller, J., Rubin-Fraenkel, M., Butkevich, A., Ginsburg, S. 1995. Oscillations in the activity of a potassium channel at the presynaptic nerve terminal. *J. Neurophysiol.* **73:**2448–2458

Rhodes, T.H., Lossin, C., Vanoye, C.G., Wang, D.W., George, A.L. Jr 2004. Noninactivating voltage-gated sodium channels in severe myoclonic epilepsy of infancy. *Proc. Natl. Acad. Sci. USA* **101:**11147–11152

Rutecki, P. A., Yang, Y. 1998. Ictal epileptiform activity in the CA3 region of hippocampal slices produced by Pilocarpine. *J. Neurophysiol.* **79:**3019–3029

Sarkar, S.N., Adhikari, A., Sikdar, S.K. 1995. Kinetic characterization of rat brain type IIA sodium channel alpha-subunit stably expressed in a somatic cell line. *J. Physiol* **488:**633–645

Schweitzer, J.S., Patrylo, P.R., Dudek, F.E. 1992. Prolonged field bursts in the dentate gyrus: dependence on low calcium, high potassium, and nonsynaptic mechanisms. *J. Neurophysiol.* **68:**2016–2025

Segal, M.M. 1994. Endogenous burst underlie seizure-like activity in solitary excitatory hippocampal neurons in microcultures. *J. Neurophysiol.* **72:**1874–1884

Shcherbatko, A., Ono, N., Mandel, G., Brehm, P. 1999. Voltage-dependent sodium channel function is regulated through membrane mechanics. *Biophys. J.* **77:**1945–1959

Sheets, M.F., Hanck, D.A. 1999. Gating of skeletal and cardiac muscle sodium channels. *J. Physiol.* **514:**425–436

Sheets, M.F., Kyle, J.W., Kallen, R.G., Hanck, D.A. 1999. The Na^+ channel voltage sensor associated with inactivation is localized to the external charged residues of domain IV, S4. *Biophys. J.* **77:**747–757

Spampanato, J., Aradi, I., Soltesz, I., Goldin, A.L. 2004a. Increased neuronal firing in computer simulations of sodium channel mutations that cause generalized epilepsy with febrile seizures plus. *J. Neurophysiol.* **91:**2040–50

Spampanato, J., Escayg, A., Meisler, M.H., Goldin, A.L. 2001. Functional effects of two voltage-gated sodium channel mutations that cause generalized epilepsy with febrile seizures plus type 2. *J. Neurosci.* **21:**7481–7490

Spampanato, J., Escayg, A., Meisler, M.H., Goldin, A.L. 2003. Generalized epilepsy with febrile seizures plus type 2 mutation W1204R alters voltage-dependent gating of Na(v)l.l sodium channels. *Neuroscience* **116:**37–48

Spampanato, J., Kearney, J.A., de Haan, G., McEwen, D.P., Escayg, A., Aradi, I., MacDonald, B.T., Levin, S.I., Soltesz, I., Benna, P., Montalenti, E., Isom, L.L., Goldin, A.L., Meisler, M.H. 2004b. A novel epilepsy mutation in the sodium channel SCN1A identifies a cytoplasmic domain for beta subunit interaction. *J. Neurosci.* **24:**10022–10034

Tammaro, P., Conti, F., Moran, O. 2002. Modulation of sodium current in mammalian cells by an epilepsy-correlated beta 1 - subunit mutation. *Biochem. Biophy. Res. Commun.* **291:**1095–1101

Toib, A., Lyakhov, V., Marom, S. 1998. Interaction between duration of activity and time course of recovery from slow inactivation in mammalian brain sodium channels. *J. Neurosci.* **18:**1893–1903

Wallace, R.H., Hodgson, B.L., Grinton, B.E., Gardiner, R.M., Robinson, R., Rodriguez-Casero, V., Sadleir, L., Morgan, J., Harkin, L.A., Dibbens, L.M., Yamamoto, T., Andermann, E., Mulley, J.C., Berkovic, S.F., Scheffer, I.E. 2003. Sodium channel alphal-subunit mutations in severe myoclonic epilepsy of infancy and infantile spasms. *Neurology* **61:**765–79

Wallace, R.H., Scheffer, I.E., Barnett, S., Richards, M., Dibbens, L., Desai, R.R., Lerman-Sagie, T., Lev, D., Mazarib, A., Brand, N., Ben-Zeev, B., Goikhman, I., Singh, R., Kremmidiotis, G., Gardner, A., Sutherland, G.R., George, A.L. Jr., Mulley, J.C., Berkovic, S.F. 2001. Neuronal sodium-channel alphal-subunit mutations in generalized epilepsy with febrile seizures plus. *Am. J. Hum. Genet.* **68:**859–865

Wallace, R.H., Wang, D.W., Singh, R., Scheffer, I.E., George, A.L. Jr, Phillips, H.A., Saar, K., Reis, A., Johnson, E.W., Sutherland, G.R., Berkovic, S.F., Mulley, J.C. 1998. Febrile seizures and generalized epilepsy associated with a mutation in the Na + - channel betal subunit gene SCN1B. *Nat. Genet.* **19:**366–370

Wang, S., Wang, G.K. 1997. A mutation in segment I-S6 alters slow inactivation of sodium channels. *Biophys. J.* **72:**1633–1640

Wu, N., Hsiao, C.F., Chandler, S.H. 2001. Membrane resonance and sub threshold membrane oscillations in mesencephalic V neurons: participants in burst generation. *J. Neurosci.* **21:**3729–3739

Yamaguchi, Y., Aota, Y., Sato, N., Wagatsuma, H., Wu, Z. 2004. Synchronization of neural oscillations as a possible mechanism underlying episodic memory: a study of theta rhythm in the hippocampus. *J. Integr. Neurosci.* **3:**143–157

Yu, F.H., Westenbroek, R.E., Silos-Santiago, I., McCormick, K.A., Lawson, D., Ge, P., Ferriera, H., Lilly, J., DiStefano, P.S., Catterall, W.A., Scheuer, T., Curtis, R. 2003. Sodium channel beta4, a new disulfide-linked auxiliary subunit with similarity to beta2. *J. Neurosci.* **23:**7577–7585

Zhang, P.C., Keleshian, A.M., Sachs, F. 2001. Voltage-induced membrane movement. *Nature* **413:**428–432